frontiers | Frontiers in Materials

TYPE Original Research
PUBLISHED 19 November 2024
DOI 10.3389/fmats.2024.1499691



OPEN ACCESS

EDITED BY
Biao Hu,
Shenzhen University, China

REVIEWED BY
Pan Wang,
Qingdao University of Technology, China
Zeyu Lu,
University of Macau, China
Xiongfei Liu,
Hebei University of Technology, China

*CORRESPONDENCE
Jiayang Zhang,
15620218044@163.com

RECEIVED 21 September 2024
ACCEPTED 28 October 2024
PUBLISHED 19 November 2024

CITATION
Ning X, Zhang J, Zhuang C, Su Q and Zhong S (2024) Investigation of the performance and life cycle assessment of alkali-activated sintered sludge-slag-based permeable concrete.
*Front. Mater.* 11:1499691.
doi: 10.3389/fmats.2024.1499691



# Investigation of the performance and life cycle assessment of alkali-activated sintered sludge-slag-based permeable concrete

Xiangbo Ning[1], Jiayang Zhang[2]*, Can Zhuang[3], Qunyong Su[4] and Shunjie Zhong[3]

[1]China MCC22 Group Corporation Ltd., Hebei, China, [2]School of Civil Engineering, Tianjin University, Tianjin, China, [3]Fujian Zhanglong Construction Investment Group Co., Ltd., Zhangzhou, Fujian, China, [4]Zhangzhou Municipal Engineering Center, Zhangzhou, Fujian, China

As urbanization continues to accelerate, the application of permeable concrete is becoming an increasingly prevalent practice. Nevertheless, the carbon dioxide emission issue associated with traditional permeable concrete cannot be overlooked. In this study, alkali-activated sintered sludge and slag were employed as raw materials to prepare alkali-activated sintered sludge-slag-based permeable concrete. The effects of sludge calcination temperature, sludge content, and binder-to-aggregate ratio on the compressive strength, porosity, and permeability coefficient of the permeable concrete were investigated through the implementation of one-way experiments. The formation mechanism of permeable concrete materials was analyzed using scanning electron microscopy-energy dispersive spectroscopy (SEM-EDS), and a carbon emission assessment was performed. The findings indicated that an increase in sludge content resulted in a notable decline in the 28-day compressive strength, accompanied by a reduction in the Ca/Si ratio of the C-A-S-H hydration products, from 1.08 to 0.35. Conversely, the carbon emission assessment demonstrated that abiotic losses declined markedly with an increase in sludge content, effectively mitigating the carbon emission burden associated with construction materials.

KEYWORDS

**alkali-activated permeable concrete, sludge, slag, formation mechanism, carbon emissions**

## 1 Introduction

Globally, the acceleration of urbanization and increase in industrial activities lead to the production of a significant amount of construction waste and industrial by-products, the disposal of which has become a serious environmental issue (Jiang et al., 2024; Duan and Wang, 2022; Sharma et al., 2023). Moreover, traditional cement has notable deficiencies in urban drainage and rainwater management (Adresi et al., 2023; Isukuru et al., 2024). Although its high strength and durability make it widely used in construction, the high carbon emissions from cement production severely limit its

environmental friendliness. The large amounts of carbon dioxide released during the cement production process not only exacerbate global warming but also make traditional permeable concrete unsustainable in addressing urban drainage challenges, particularly in managing rainwater permeation and reducing surface runoff. The high carbon footprint of traditional cement contradicts its environmental requirements, necessitating the search for greener alternatives (Zaid et al., 2024; Basyouni and Mahmoud, 2024; Khan and McNally, 2024).

Permeable concrete is a special type of concrete material characterized by high permeability due to large voids between aggregates, which effectively reduces surface runoff, alleviates the burden on urban drainage systems, and quickly eliminates standing water, thus mitigating urban flooding issues (Pour et al., 2020). Additionally, it aids in groundwater recharge, improves water quality, and helps alleviate urban heat island effects, providing a comfortable living environment for citizens (Florentin et al., 2024; Al Jurdi et al., 2023). This material is widely used in parking lots, sidewalks, and pathways, with relatively simple construction and maintenance requirements (Rumbach et al., 2022). However, the high cement content in traditional permeable concrete leads to significant carbon emissions, which is a pressing issue in the current global environmental context. To further reduce environmental impacts, improvements in material formulations and production processes are needed to find more sustainable solutions (Wu et al., 2024; Salami et al., 2024).

Sludge and slag are two widely available and potential supplementary cementitious materials, whose application not only helps in resource recycling but also significantly reduces the carbon footprint of building materials (Yang et al., 2024). Sludge mainly comes from urban sewage treatment plants and is a solid waste precipitated during the sewage treatment process. It contains a large amount of minerals (such as silicates, bauxite, and iron ores) and organic matter. Its chemical composition allows it to exhibit good cementitious properties when properly treated (Guo et al., 2024). By drying, crushing, and chemically processing sludge, it can be transformed into a reactive material. This material can chemically react with alkaline solutions in alkali-activated reactions, forming high-strength gel bodies, thereby partially replacing traditional cement, reducing reliance on cement, and effectively reducing waste (Zhao et al., 2024; Jin et al., 2024). Studies have explored ultra-fine kaolin, water glass, and sodium hydroxide for alkali activation, with different amounts of accelerators to produce optimal geopolymer composite materials. The results indicated that at an accelerator amount of 5%, the geopolymer exhibited the best apparent density, porosity, and enhancement effects, and the strength of geopolymers with accelerators was higher than those without when the accelerator dosage was increased within a certain range. Slag is a by-product of the metallurgical industry, mainly originating from the smelting of iron ores and other metal ores (Đorđević et al., 2024). The slag produced during smelting is rich in silicates, bauxite, and lime, which exhibit good cementitious properties after grinding. Slag can also react with alkaline solutions to form a high-strength and stable cementitious material, making it an eco-friendly alternative material in construction engineering, reducing the use of traditional cement (Cui et al., 2024).

Meanwhile, sludge and slag are ideal precursors for alkali-activated reactions. Alkali-activated reactions utilize strong alkaline solutions (such as sodium hydroxide or calcium hydroxide) to activate the minerals in these materials, forming high-performance cementitious products. These alkali-activated products exhibit excellent physical and chemical properties, including high strength, low permeability, and good chemical corrosion resistance (Yuan et al., 2024). Studied the effects of different cement and alkali contents on the mechanical properties of cementitious materials. Their research indicated that increasing the amounts of cement and alkali led to higher strength in the cementitious materials (Yu et al., 2024). Notably, variations in alkali content had a more pronounced effect on the early strength of the materials. However, when the cement content exceeded 10%, the mechanical properties began to decline. By this method, sludge and slag can be converted into effective building materials, greatly reducing the demand for traditional cement, thus lowering the carbon emissions during the production of building materials and promoting the development of sustainable building materials (Kuoribo et al., 2024). Although alkali-activated materials have shown good application prospects in the construction industry, research on alkali-activated permeable concrete is still relatively limited. Most existing studies focus on the performance and environmental impacts of traditional permeable concrete, lacking in-depth discussions on alkali-activated permeable concrete, and research on aspects such as life cycle assessment of alkali-activated permeable concrete is not yet complete (Salami et al., 2024).

This paper mainly investigates the effects of sludge calcination temperature, the content of sintered sludge, and the aggregate-to-binder ratio on the compressive strength, connectivity porosity, and permeability coefficient of alkali-activated permeable concrete. It also analyzes the formation mechanism of the permeable concrete material using scanning electron microscopy-energy dispersive spectroscopy (SEM-EDS) testing methods. Additionally, a life cycle assessment (LCA) study is conducted to explore its environmental impact. By systematically evaluating the mechanical properties, permeability, and durability of alkali-activated sintered sludge-slag-based permeable concrete, this research aims to provide a scientific basis for its application in urban infrastructure. Furthermore, this study will combine the LCA method to comprehensively analyze the environmental impact of this material, thus offering theoretical support and practical guidance for the development and application of green building materials.

# 2 Materials and methods

## 2.1 Raw materials

The sludge used in this study was sourced from Baiyangdian in Hebei, while the slag was obtained from a steel mill in Hunan. The main components include $SiO_2$, CaO, and $Al_2O_3$, as shown in Table 1. The coarse aggregate used was ordinary limestone crushed stone with a particle size of 4.75–9.5 mm from the Hengji Stone Factory in Jilin City. The particle grading, particle size, mud content, crushing index, and void ratio of the coarse aggregate all meet the requirements of the "Pebbles and Crushed Stone for Building Use" (GB/T 14685-2022) and "Technical Specifications for Permeable Cement Concrete Pavement" (CJJ/T 135-2009) (Zhang et al., 2024). The water glass solution came from a chemical plant in Handan,

TABLE 1 Chemical composition of sludge.

| Oxide (%) | CaO | $SiO_2$ | $Al_2O_3$ | $Fe_2O_3$ | $SO_3$ | MgO | $K_2O$ | $TiO_2$ |
|---|---|---|---|---|---|---|---|---|
| Sludge | 6.25 | 58.95 | 19.01 | 6.27 | 0.28 | 2.75 | 2.96 | 0.82 |
| Slag | 39.23 | 35.56 | 15.45 | 0.71 | 4.22 | 8.21 | 0.45 | 0.82 |

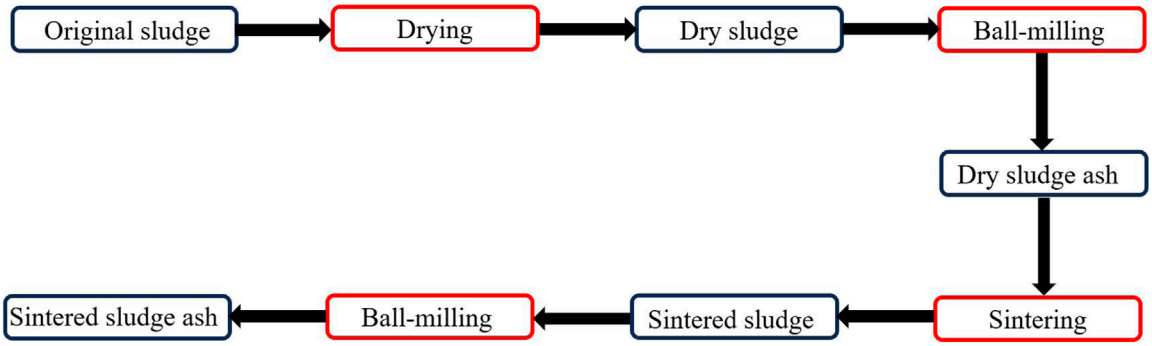


FIGURE 1
The calcination activation process of sludge.

Hebei Province, with a modulus of 3.1, a $SiO_2$ mass fraction of 27.54%, and a $Na_2O$ mass fraction of 9.35%. Solid sodium hydroxide, with a purity of 98.9%, was sourced from a chemical plant in Luoyang, Henan Province.

## 2.2 Mix proportion design

Preliminary experiments were conducted to explore the characteristics of the raw materials and the performance requirements of the permeable concrete to be satisfied, and the general range for the alkali equivalence and the sludge to slag ratio was determined. In the experiments, the water to binder ratio was fixed at 0.4, the modulus of the water glass was consistently 3.1 M, and the alkali content referred to the percentage of $Na_2O$ in the total mass of sludge and slag.

The sludge was treated by calcination: first, the sludge blocks were placed in an oven and dried at 150°C. The dried blocky sludge was then ground in a ball mill for 6 min to produce powdered sludge ash. The sludge ash was then placed in a crucible and calcined in a high-temperature furnace, heating at a rate of 10°C/min to temperatures of 400°C, 600°C, and 800°C, then held at these temperatures for 120 min to produce sintered sludge, which was finally ground again for 1 min to obtain sintered sludge ash. As shown in Figure 1.

Using the volumetric method to determine the mix ratio of permeable concrete, the speccific steps are as shown in Equations 1–3:

$$\frac{m_s}{\rho_s}+\frac{m_r}{\rho_r}+\frac{m_w}{\rho_w}+\frac{m_a}{\rho_a}+\frac{m_g}{\rho_g}=1 \quad (1)$$

$$\frac{m_w}{m_r+m_s}=0.4 \quad (2)$$

$$\frac{m_r+m_s}{m_g}=0.24 \quad (3)$$

where $m_s$ is the mass of the slag in a dry state (g), $m_r$ is the mass of the slag in a dry state (g), $m_w$ is the mass of water (g), $m_a$ is the mass of the alkaline activator (g), $m_g$ is the mass of coarse aggregate (g), $\rho_s$ is the density of the slag in a dry state (g/cm$^3$), $\rho_r$ is the density of the slag in a dry state (g/cm$^3$), $\rho_w$ is the density of water (g/cm$^3$), $\rho_a$ is the density of the alkaline activator (g/cm$^3$), $\rho_g$ is the density of the coarse aggregate in a bulk state (g/cm$^3$).

The experiment was designed with sludge undergoing no calcination treatment and calcination at different temperatures: 400°C, 600°C, 800°C. The sludge content was: 0%, 10%, 30%, 50%, and different binder-aggregate ratios: 0.2, 0.22, 0.24, 0.26, resulting in a total of 12 experimental groups. The experimental mix ratio design is shown in Table 2.

## 2.3 Specimen preparation

The concrete mix was prepared using a two-charge method, tamped into molds to form 100 mm × 100 mm × 100 mm non-standard test blocks. Sodium hydroxide, water glass, and water were mixed to prepare different moduli of alkali activators, which were then stored indoors to cool for 24 h before use. The pre-moistened coarse aggregate was first put into the mixer, followed by 20%–30% alkali activator solution and mixed for 30 s to ensure the coarse aggregate was sufficiently wet to better adhere to the cementitious materials, then, the pre-mixed sludge and slag were added and mixed for 1 min to evenly coat the aggregate surfaces with cementitious materials, finally, the remaining alkali activator solution was added and mixed for 3 min to fully coat the aggregate. The mixture was loaded in two layers, tamped, and then cured in still water until the age for performance testing.

10.3389/fmats.2024.1499691

TABLE 2 Experimental mix ratios.

| Number | Sludge | | Slag ($kg/m^3$) | Aggregate ($kg/m^3$) | Alkali concentratio ($kg/m^3$) | Water ($kg/m^3$) | Binder-to-aggregate ratio ($kg/m^3$) |
|---|---|---|---|---|---|---|---|
| | Temperature (°C) | Content ($kg/m^3$) | | | | | |
| T1 | 20 | 83.11 | 193.93 | 1154.46 | 16.62 | 96.96 | 0.24 |
| T2 | 400 | 83.11 | 193.93 | 1154.46 | 16.62 | 96.96 | 0.24 |
| T3 | 600 | 83.11 | 193.93 | 1154.46 | 16.62 | 96.96 | 0.24 |
| T4 | 800 | 83.11 | 193.93 | 1154.46 | 16.62 | 96.96 | 0.24 |
| S1 | 600 | 0.00 | 280.37 | 1168.33 | 16.82 | 98.13 | 0.24 |
| S2 | 600 | 27.92 | 251.33 | 1163.67 | 16.75 | 97.74 | 0.24 |
| S3 | 600 | 83.11 | 193.93 | 1154.46 | 16.62 | 96.96 | 0.24 |
| S4 | 600 | 137.43 | 137.43 | 1145.39 | 16.49 | 96.20 | 0.24 |
| L1 | 600 | 71.90 | 167.77 | 1198.37 | 14.38 | 83.88 | 0.20 |
| L2 | 600 | 77.62 | 181.11 | 1175.97 | 15.52 | 90.55 | 0.22 |
| L3 | 600 | 83.11 | 193.93 | 1154.46 | 16.62 | 96.96 | 0.24 |
| L4 | 600 | 88.42 | 206.33 | 1133.65 | 17.68 | 103.16 | 0.26 |

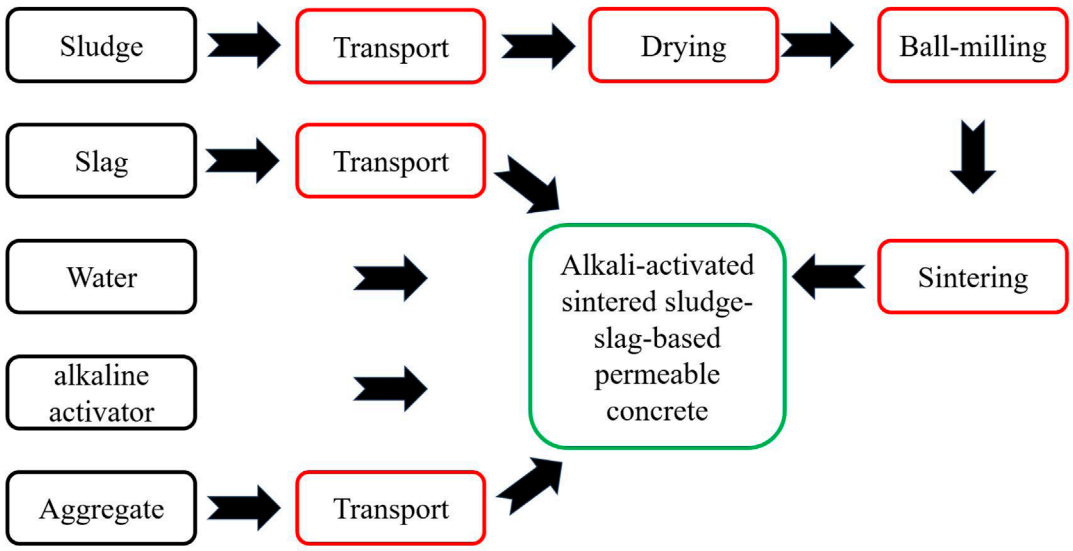


FIGURE 2
System boundary for alkali-activated sintered sludge-slag permeable concrete.

## 2.4 Experimental methods

### 2.4.1 Compressive strength

The compressive strength of the specimens was tested using a YAW-300C fully automatic compression testing machine produced by Jinan Shidai Test Gold Testing Machine Co., Ltd., following the standards in GB/T 50081-2019 "Standard for Test Methods of Physical and Mechanical Properties of Concrete." The cured alkali-activated sintered sludge-slag-based permeable concrete blocks were placed on the platform of the testing machine, ensuring good contact between the bottom of the sample and the platform surface. During the compressive strength test, the loading speed was adjusted to 2.4 kN/s. The data recorded were processed by arithmetic average to calculate the compressive strength of the group. If

10.3389/fmats.2024.1499691

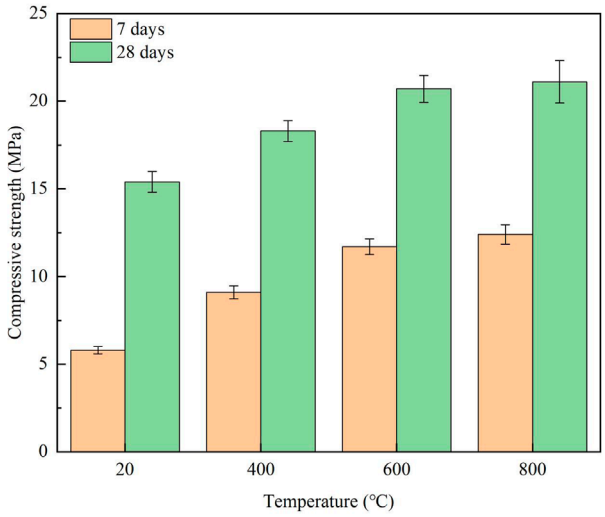


FIGURE 3
Effect of sludge calcination temperature on compressive strength.

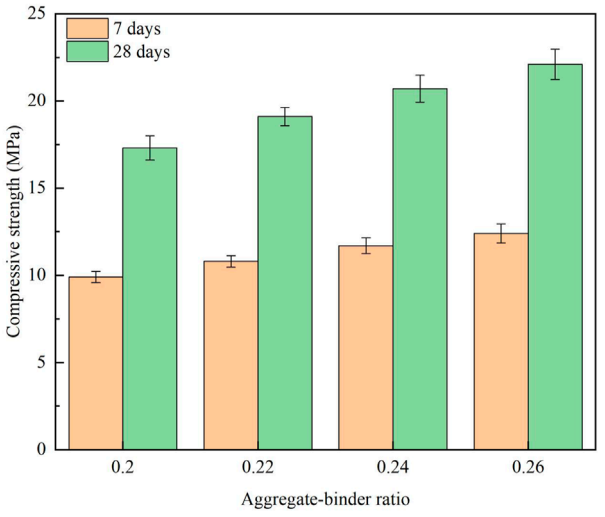


FIGURE 5
Effect of different binder-to-aggregate ratios on compressive strength.

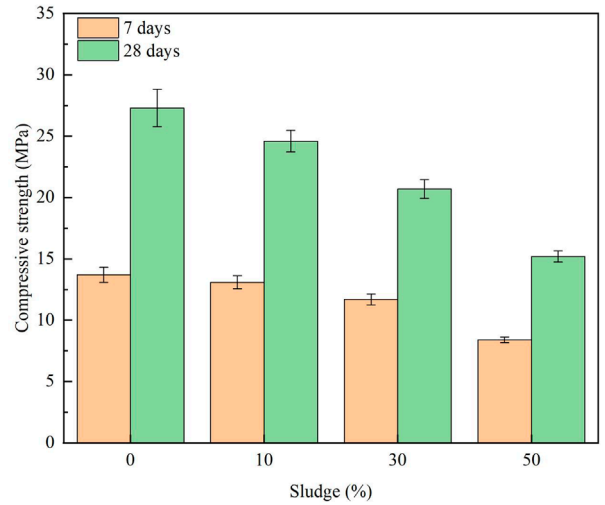


FIGURE 4
Effect of sludge content on compressive strength.

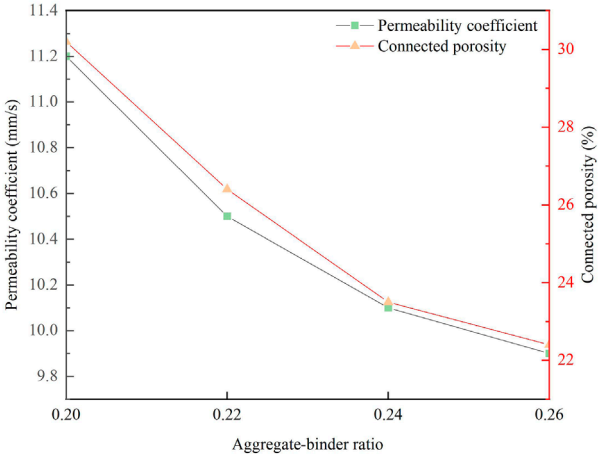


FIGURE 6
Effect of different binder-to-aggregate ratio on porosity and permeability coefficient.

the experimental values in the group had large errors, they were processed again.

### 2.4.2 Permeability coefficient

The permeability coefficient was tested according to CJJ/T135-2009 (Muauz et al., 2024). The sample size for testing was a cylinder with a base diameter of 100 mm and a height of 50 mm. Calculated according to Equation 4:

$$K_T = \frac{QL}{AHt} \tag{4}$$

where $KT$ is the permeability coefficient (mm/s), $T$ is the water temperature (°C), $Q$ is the volume of water collected in t s ($mm^3$), $L$ is the thickness of the specimen (mm), $A$ is the surface area of the specimen ($mm^2$), $H$ is the water level difference (mm), and $t$ is the time (s).

### 2.4.3 Connected porosity rate

The test for connected porosity rate of permeable concrete specimens was used to evaluate the connectivity of the pores and the overall permeability. Firstly, the permeable concrete specimens, sized 100 mm × 100 mm × 100 mm, were cured under standard conditions for 28 days. After reaching the age, the specimens were placed in an oven and dried to constant weight at a set temperature of (105 ± 5)°C. After removal, the specimens were cooled to room temperature in a cool, dry environment and weighed. Then, they were immersed in water, treated to saturation until no more bubbles emerged from the surface. Following this, the saturated specimens were weighed in water, and their mass was recorded. By comparing

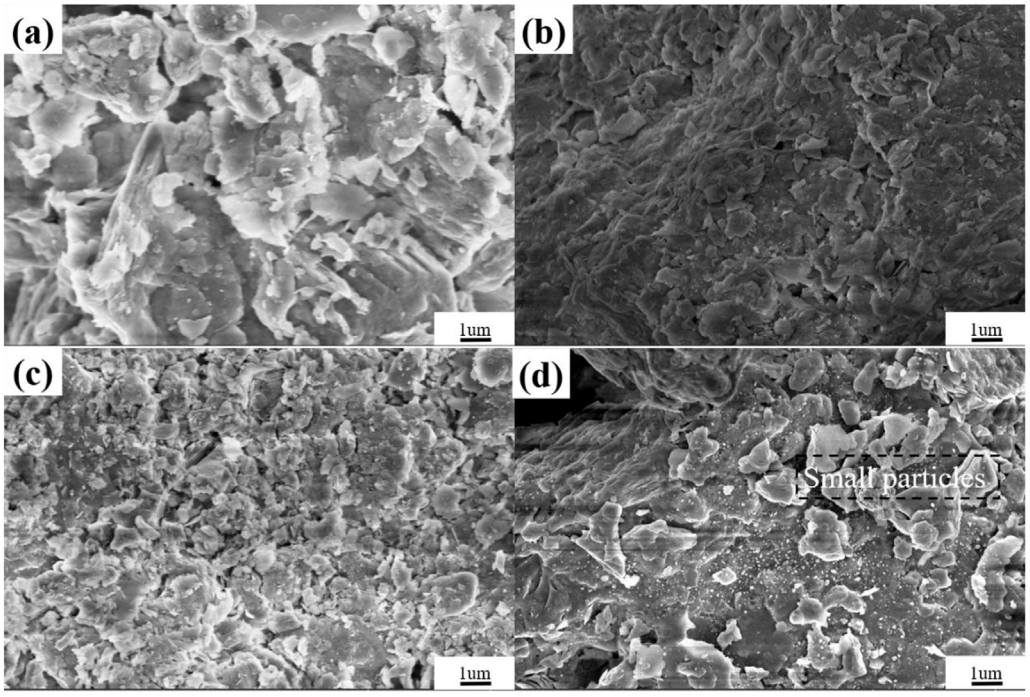


FIGURE 7
Morphology of alkali-activated sintered sludge-slag-based permeable concrete at different temperatures. **(A)** 20°C **(B)** 400°C **(C)** 600°C **(D)** 800°C.

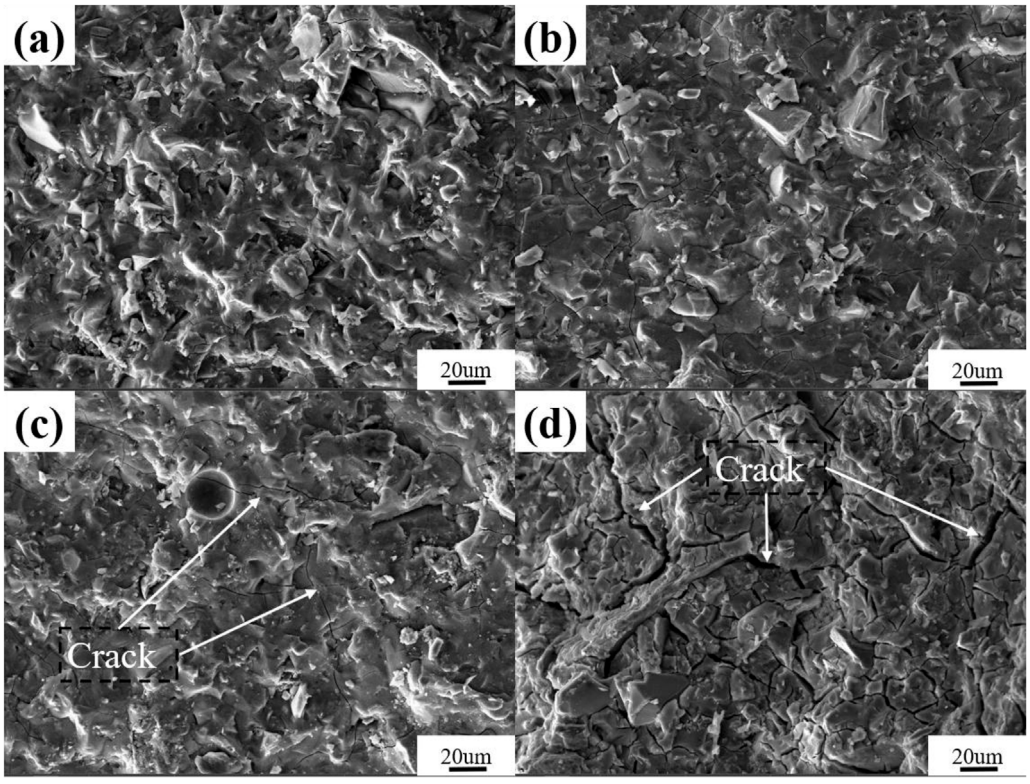


FIGURE 8
Morphology of alkali-activated slag permeable concrete with different content of sintered sludge. **(A)** 0% **(B)** 10% **(C)** 30% **(D)** 50%.

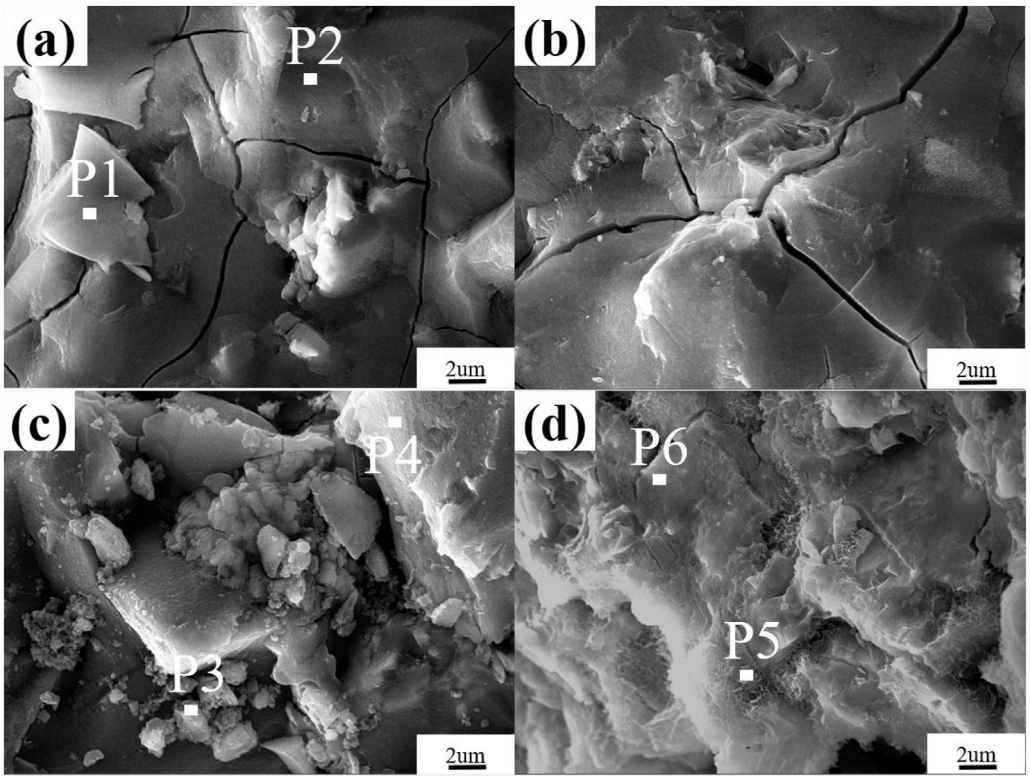


FIGURE 9
Morphology of alkali-activated slag permeable concrete with different amounts of sintered sludge at high magnification. **(A)** 0.20 **(B)** 0.22 **(C)** 0.24 **(D)** 0.26.

the mass of the specimen in the dry state with the mass in the saturated state, the connected porosity can be calculated. Calculated according to Equation 5:

$$P = \left(1 - \frac{m_1 - m_2}{\rho V}\right) \times 100\% \quad (5)$$

where $P$ is the connected porosity rate (%), $m_1$ is the mass of the specimen in dry state (g), $m_2$ is the mass of the specimen in saturated state (g), $\rho$ is the density of the specimen (g/cm$^3$), and $V$ is the volume of the specimen (cm$^3$).

### 2.4.4 Scanning electron microscope (SEM)

To observe the microstructure and elemental composition of the hydration products in the alkali-activated sintered sludge-slag-based permeable concrete, a Quanta 250 Field Emission Scanning Electron Microscope (FEI/SEM, Hillsboro, OA, United States) was used. Due to the poor conductivity of the alkali-activated sintered sludge-slag-based permeable concrete, it was necessary to apply conductive adhesive to the sample surface first, followed by gold sputtering to enhance the sample's conductivity.

### 2.4.5 Life cycle assessment method (LCA)

Life Cycle Assessment (LCA) is a method for analyzing and evaluating the overall resource inputs and emissions outputs throughout the entire lifecycle of a product. This includes everything from raw material extraction, transportation, and processing to the final product's use and eventual disposal (Liang et al., 2024). The assessment process consists of four main components: defining the goal and scope, inventory analysis, impact assessment, and interpretation of the lifecycle results.

In this experiment, the LCA model aimed to quantify the resource and environmental impacts of producing alkali-activated sintered sludge-slag permeable concrete under various material proportions. The research findings will provide substantial evidence and reference for selecting sludge treatment conditions in terms of resource and environmental impacts, aiding decision-making when related research is implemented in real production (Tamoor et al., 2023).

When discussing the standard scope, it is essential to highlight that the majority of moisture in the sludge drying phase is lost during natural air drying. Given sufficient time, this process can even result in complete dryness. The treatment of specimens in an oven was not included in the primary conditions under consideration, as its energy consumption is relatively low compared to the overall process, leading to minimal environmental impact. Consequently, the cut-off principle was applied to exclude this process.

In summary, the system boundary for the production of alkali-activated sintered sludge-slag permeable concrete is illustrated in Figure 2.

This experiment utilizes SimaPro as the software tool for constructing the life cycle assessment model (Herrando et al., 2022). Developed by the Centre for Environmental Science at Leiden University in the Netherlands, SimaPro is currently used in over 80 countries. The software includes a rich set of databases, such as large databases like ecoinvent, ELCD, the U.S. Life Cycle Inventory Database, and the IDEA Japan Inventory Database, as

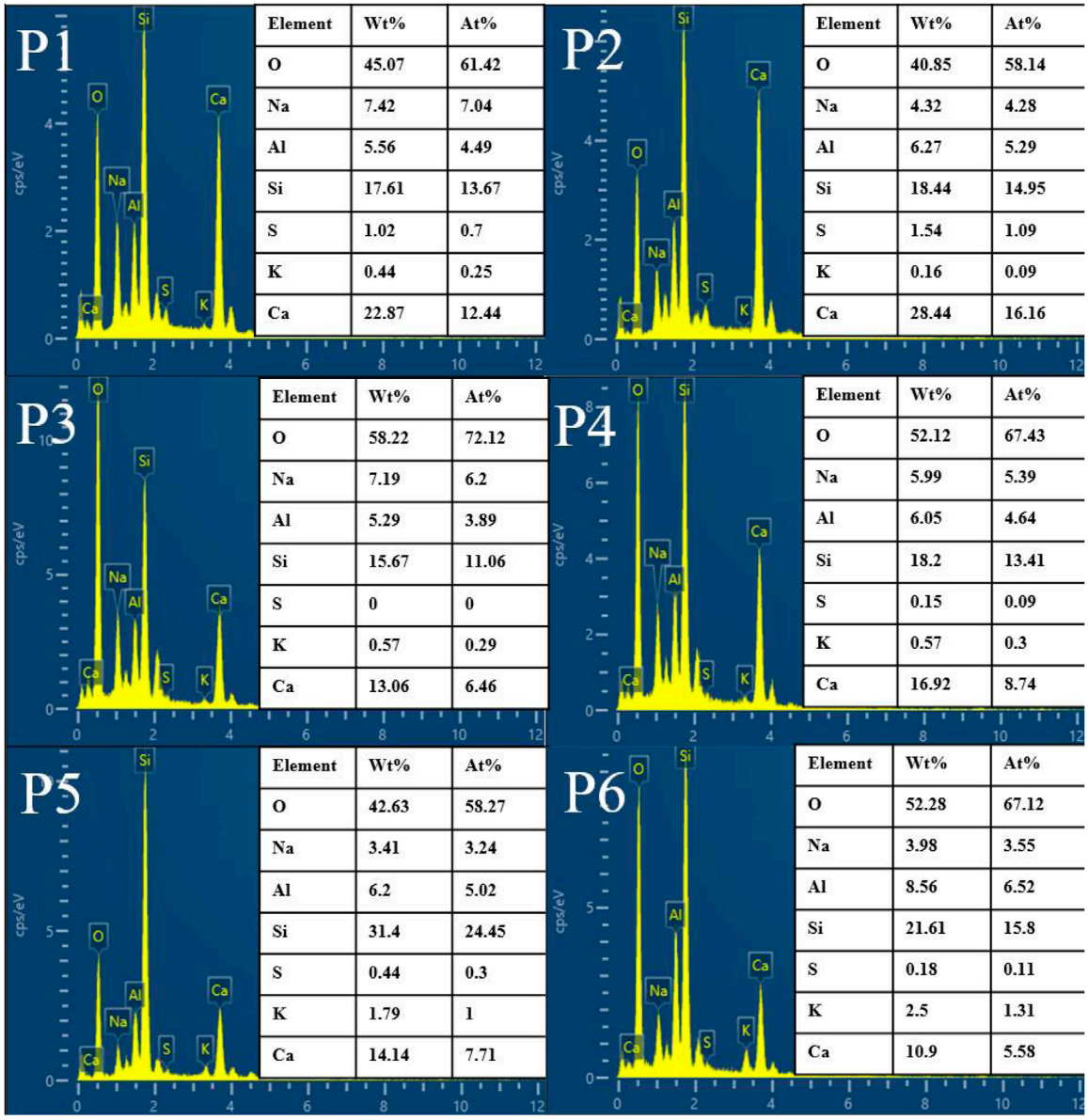


FIGURE 10
EDS energy spectrum analysis of alkali-activated slag permeable concrete with different content of sintered sludge.

well as numerous industry-specific databases like PlasticsEurope, ERASM, and World Steel. The databases related to construction materials, transportation processes, and treatment methods are relatively comprehensive and sufficient to meet the requirements for building the corresponding model.

# 3 Results and discussion

## 3.1 Compressive strength analysis

### 3.1.1 Sludge calcination temperature

Figure 3 showed the compressive strength of permeable concrete at 7 and 28 days under room temperature and various calcination temperatures (20°C, 400°C, 600°C, 800°C) (Yan et al., 2022). It was observed that as the calcination temperature of sludge increases, so did the compressive strength of the permeable concrete. This increase in strength was due to the reduction of organic substances within the sludge, which would otherwise impede hydration reactions and affect the strength of the concrete. The structural changed in the sludge particles after calcination also made them more conducive to bonding with the cement matrix, thereby enhancing the overall strength of the concrete. The influence of temperature on strength showed a more pronounced effect in the early stages, becoming nearly consistent at higher temperatures. At 600°C, almost all organic materials were decomposed, hence the impact on the strength of sludge at 600°C and 800°C was nearly the same.

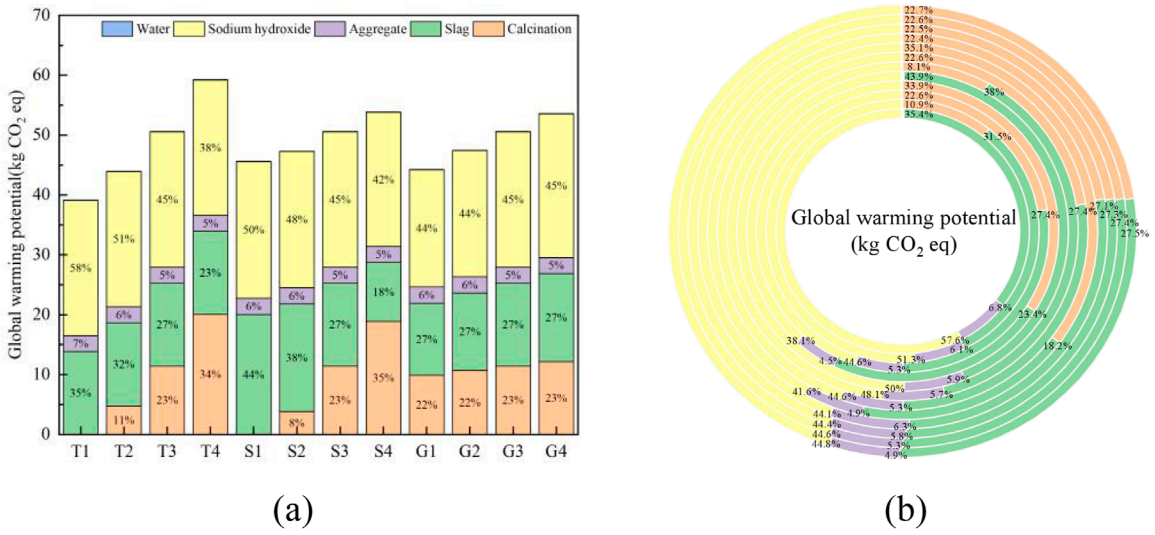


FIGURE 11
The **(A)** eigenvalue and **(B)** composition ratio of GWP.

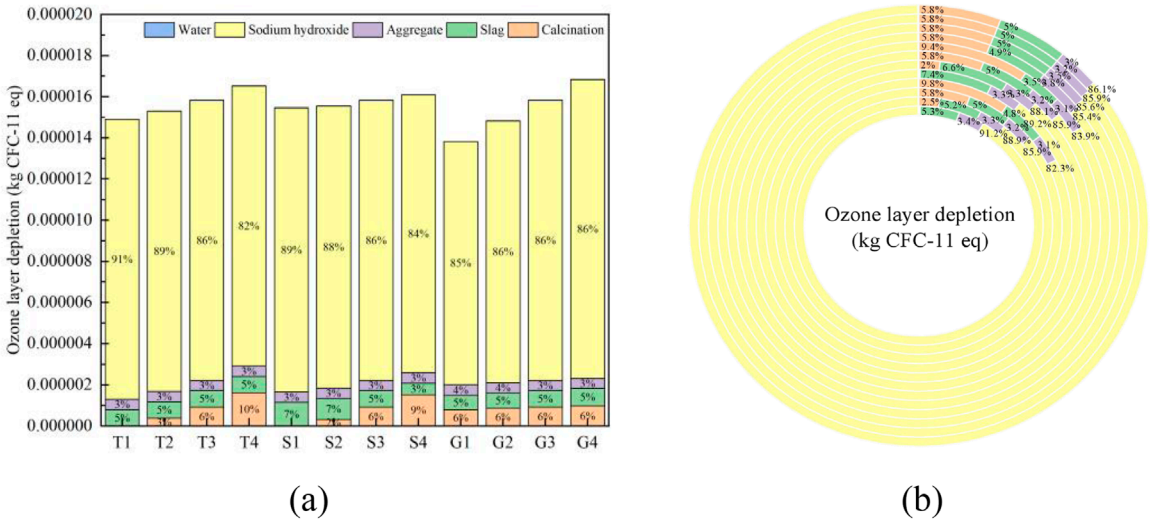


FIGURE 12
The **(A)** eigenvalue and **(B)** composition ratio of OLDP.

### 3.1.2 Sintered sludge content

Figure 4 illustrated the compressive strength of permeable concrete at 7 and 28 days with different sintered sludge contents (0%, 10%, 30%, 50%). As the sintered sludge content increases, the compressive strength of the permeable concrete decreases. This was because sludge, as an auxiliary cementitious material, offers lower strength than slag. When the sludge contents of 0%–30%, the strength at 7 days changed little, while at 28 days, the strength significantly reduced, indicating that sludge contributes more to the early strength, whereas slag provides better late strength. It was evident that at a sludge content of 50%, there is a sharp drop in strength. This may be due to excessive sludge content reducing the flowability of the permeable concrete, making it difficult to compact during preparation, and creating weak areas, thereby reducing the compressive strength of the concrete. Therefore, sludge content should ideally be kept within 50%.

### 3.1.3 Binder-to-aggregate ratio

Figure 5 showed the compressive strength of permeable concrete at 7 and 28 days with different binder-to-aggregate ratios (0.2, 0.22, 0.24, 0.26). As the binder-to-aggregate ratio increased, so did the strength at both 7 and 28 days, although the increase was relatively modest. Additionally, the 28 days strength was approximately twice that of the 7 days compressive strength. When the

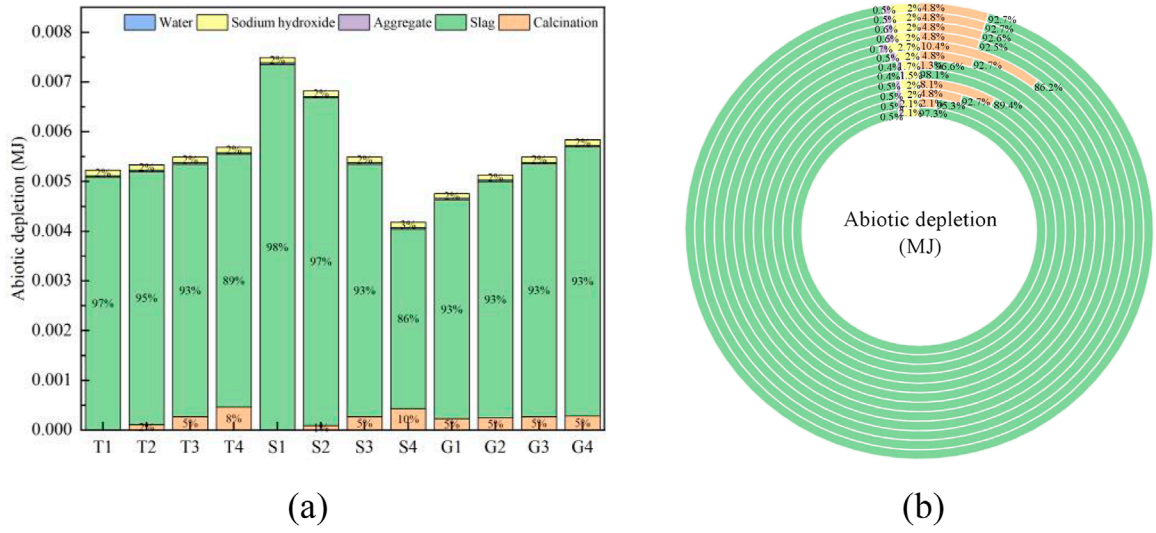


FIGURE 13
The **(A)** eigenvalue and **(B)** composition ratio of ADP.

binder-to-aggregate ratio was low, the cementitious material provided a weaker coating around the aggregates, and the coating layer was thinner. Also, due to more aggregates, the cementitious material may accumulate in clumps, failing to adequately bond all aggregates, thus resulting in lower compressive strength. As the amount of cementitious material increased, both the degree of coating around aggregates and the thickness of the coating improve, and the reduction in aggregate quantity allows the cementitious material to better connect all aggregates, enhancing the compressive strength of the permeable concrete.

### 3.1.4 Connected porosity and permeability analysis

Figure 6 shows the effect of different binder-to-aggregate ratio on porosity andpermeability coefficient. Comparing the connected porosity and permeability coefficients, a similar trend can be observed, both decreasing as the binder-to-aggregate ratio increases, with the rate of decrease slowing as the ratio increases (Liu et al., 2022). This was because the primary channels for water permeability in permeable concrete were the voids between aggregates rather than the cementitious material itself, thus there was a strong correlation between connected porosity and permeability coefficients. At lower binder-to-aggregate ratios, due to inadequate coating of aggregates by cementitious materials, the connections between aggregates were poor, resulting in more pores. This resulted in higher connected porosity and permeability coefficients. As the cementitious material fully enveloped the aggregates, this phenomenon gradually diminished, significantly reduced both metrics (Shanmuganathan et al., 2023).

## 3.2 Microscopic morphology

Figure 7 shows the alkali-activated permeable concrete composed of sintered sludge and slag as precursor materials at different calcination temperatures. It is evident that as the calcination temperature increases, the minerals gradually decompose, forming more fine particles. High-temperature calcination activation enhances the reactivity of sludge, contributing to improved strength and durability of permeable concrete (Wang et al., 2024). Moreover, the higher the temperature, the denser the microstructure, forming a more compact network structure, which aids in the mechanical performance of the permeable concrete. However, at 800°C, increased porosity and a looser particle structure were observed, which may be due to recrystallization (Tiwari et al., 2020).

Figure 8 shows the alkali-activated slag permeable concrete with different proportions of sintered sludge at 28 days of age. As the sludge content increased, cracks and pores become more apparent within the cementitious material, indicating that the addition of sintered sludge inhibits the shrinkage ability of the alkali-activated cementitious material. The primary hydration products in the alkali-activated slag reaction are calcium-aluminosilicate hydrates (C-A-S-H) and calcium-aluminate hydrates (C-A-H). C-A-S-H possesses good binding properties, while calcium-aluminate hydrates (C-A-H) formed in a high-alkali environment when aluminum in slag reacted with calcium, enhancing the material's strength and durability (Kosar et al., 2023). Hydration products typically appeared as irregular granular or gel-like structures, which interlace during hydration to form complex networks. The compactness of the alkali-activated slag cementitious material was typically higher. However, the early high hydration degree of alkali-activated cementitious materials can adversely affect the material of sustained development, sludge addition balances the excessive early reaction of slag, achieving the goal of sustained development for permeable concrete cementitious materials (Zhu et al., 2024).

As shown in Figure 9, high-magnification images reveal unreacted calcined sludge particles at point P3 in samples with high sludge content, as evidenced by the spectrum in Figure 10. This

observation indicates that the calcined sludge has not been fully decomposed, suggesting that its reactivity is lower than that of the slag. This incomplete decomposition may result from insufficient processing conditions or inadequate exposure time during the calcination process.

Through the energy spectrum of 2, 4, 6 points in Figure 10, it was found that the content of calcined sludge is from 0% to 30% to 50%, and the Ca/Si of hydration product C-A-S-H was from 1.08 to 0.65 to 0.35. The results were consistent with the high silicon content of calcined sludge. The addition of calcined sludge changed the structure of hydration products and reduced its Ca/Si.

## 3.3 Life cycle assessment

### 3.3.1 Global warming potential (GWP)

Global warming potential indicates the likelihood of global warming over 100 years, mainly related to greenhouse gas emissions as shown in the Figure 11. The metric is expressed in kg $CO_2$ eq. The results showed that the main sources were sodium hydroxide and slag, and as the calcination temperature increased, the impact of calcination also rised (Yan et al., 2022). Considering the effects of calcination temperature on mechanical properties, it was advisable to avoid calcination temperatures above 800°C. Excessive calcination temperatures not only minimally enhance mechanical properties but can also negatively impact the environment. Additionally, as the sludge content increases, the global warming potential also rises, although the changes were minor at lower sludge contents (10%).

### 3.3.2 Ozone layer depletion

Ozone layer depletion refers to the gradual thinning of Earth's upper atmosphere ozone layer caused by the release of gaseous chlorine or bromine compounds from industrial and other human activities as shown in the Figure 12. The metric is expressed in kg CFC-11 eq (Pradel et al., 2021; Savinykh et al., 2021). As observed, ozone layer depletion slowly increases with higher calcination temperatures due to the destructive effects of the calcination process on the ozone layer. Using sludge in place of slag almost does not change the ozone layer depletion, signifying that substituting slag with sludge can manage solid waste without adding to the destruction of the ozone layer. As the binder-to-aggregate ratio increases, leading to higher usage of cementitious materials, ozone layer depletion also rises (Wang et al., 2023).

### 3.3.3 Abiotic depletion (fossil fuels)

Abiotic depletion indicates the consumption of non-renewable resources such as fossil fuels, measured in MJ, as shown in the Figure 13 (Wang et al., 2023). With increasing calcination temperature, there is little change in abiotic depletion. However, as the replacement amount of sludge increases, there is a significant decline. At a 50% substitution level, abiotic depletion decreases by nearly 50%. This is primarily because the main source of abiotic depletion is slag, thus, reducing the amount of slag significantly lowers abiotic depletion. Without compromising mechanical strength, increasing the sludge substitution amount can effectively reduce abiotic depletion (Burchart-Korol, 2013).

# 4 Conclusion

This study provides an in-depth exploration of the performance and life cycle of alkali-activated sintered sludge-slag permeable concrete, leading to the following important conclusions:

(1) Mechanical performance: As the calcination temperature of the sludge increases, the compressive strength of the permeable concrete correspondingly rises. This improvement is primarily attributed to the synergistic effect between the sintered sludge and slag, which forms a stable three-dimensional network structure. However, with an increase in sludge content, the compressive strength decreases because the strength provided by the sludge as an auxiliary binder is lower than that of the slag.

(2) Microscopic features: As the sintering temperature continues to rise, minerals gradually decompose, generating more fine particles. High-temperature calcination activation allows the sludge to exhibit better reactivity, contributing to enhanced strength and durability of the permeable concrete. However, with an increase in sludge content, cracks appear in the binder material, leading to increased porosity, while the calcium-to-silicon ratio of the hydration products initially increases and then decreases.

(3) Environmental impact: Reducing the amount of slag can significantly lower abiotic depletion. At the same time, an increase in sludge content leads to a rise in global warming potential, although the variation is relatively small at lower substitution levels (10%).

Future research can focus on further optimizing the ratio of sintered sludge to slag to achieve the best mechanical performance and economic benefits, particularly in balancing the relationship between sludge content and compressive strength. Additionally, exploring the impact of different sintering temperatures on material properties is crucial for enhancing the long-term durability of permeable concrete. Lastly, while reducing the slag content can significantly decrease abiotic depletion, increasing sludge content raises global warming potential, thus, it is necessary to seek more environmentally friendly material alternatives or additives to mitigate environmental impacts.

# Data availability statement

The original contributions presented in the study are included in the article/supplementary material, further inquiries can be directed to the corresponding author.

# Author contributions

XN: Investigation, Methodology, Resources, Validation, Writing–original draft, Writing–review and editing. JZ:

Conceptualization, Data curation, Formal Analysis, Resources, Visualization, Writing–original draft, Writing–review and editing. CZ: Conceptualization, Formal Analysis, Methodology, Validation, Writing–original draft. QS: Data curation, Formal Analysis, Investigation, Software, Writing–original draft. SZ: Funding acquisition, Investigation, Project administration, Software, Writing–original draft.

## Funding

The author(s) declare financial support was received for the research, authorship, and/or publication of this article. Financial support from the National Natural Science Foundation of Tianjin under the grants of 21JCZDJC00410 is gratefully acknowledged.

## Conflict of interest

Author XN was employed by China MCC22 Group Corporation Ltd. Authors CZ and SZ were employed by Fujian Zhanglong Construction Investment Group Co., Ltd.

The remaining authors declare that the research was conducted in the absence of any commercial or financial relationships that could be construed as a potential conflict of interest.

## Publisher's note



## References

Adresi, M., Yamani, A., Karimaei Tabarestani, M., and Rooholamini, H. (2023). A comprehensive review on pervious concrete. *Constr. Build. Mater.* 407, 133308. doi:10.1016/j.conbuildmat.2023.133308

Al Jurdi, M., Wehbe, R., and Mroueh, H. (2023). Integration of citizens' feelings and feedback into the city information modeling environment. *Sustain. Cities Soc.* 99, 104971. doi:10.1016/j.scs.2023.104971

Basyouni, Y. A., and Mahmoud, H. (2024). Affordable green materials for developed cool roof applications: a review. *Renew. Sustain. Energy Rev.* 202, 114722. doi:10.1016/j.rser.2024.114722

Burchart-Korol, D. (2013). Life cycle assessment of steel production in Poland: a case study. *J. Clean. Prod.* 54, 235–243. doi:10.1016/j.jclepro.2013.04.031

Cui, W., Liu, J., Duan, W., Xie, M., Li, X., and Dong, X. (2024). Study on the synergistic effects and eco-friendly performance of red mud-based quaternary cementitious materials. *Constr. Build. Mater.* 428, 136352. doi:10.1016/j.conbuildmat.2024.136352

Đorđević, T., Tasev, G., Aicher, C., Potysz, A., Nagl, P., Lengauer, C. L., et al. (2024). Mineralogy and environmental stability of metallurgical slags from the Euronickel smelter, Vozarci, North Macedonia. *Appl. Geochem.* 170, 106068. doi:10.1016/j.apgeochem.2024.106068

Duan, L., and Wang, L. (2022). How does the construction of China's ecological civilization affect the health burden of urban and rural residents? *Chin. J. Popul. Resour. Environ.* 20 (4), 369–382. doi:10.1016/j.cjpre.2022.11.007

Florentin, K. M., Onuki, M., and Yarime, M. (2024). Facilitating citizen participation in greenfield smart city development: the case of a human-centered approach in Kashiwanoha international campus town. *Telematics Inf. Rep.* 15, 100154. doi:10.1016/j.teler.2024.100154

Guo, K., Li, Y., Wang, J., Sui, Z., Wang, T., and Pan, W.-P. (2024). A review on selenium in coal-fired power plants: content and forms in coal, determination methods, migration, transformation, and control technologies. *J. Environ. Chem. Eng.* 12 (5), 113579. doi:10.1016/j.jece.2024.113579

Herrando, M., Elduque, D., Javierre, C., and Fueyo, N. (2022). Life Cycle Assessment of solar energy systems for the provision of heating, cooling and electricity in buildings: a comparative analysis. *Energy Convers. Manag.* 257, 115402. doi:10.1016/j.enconman.2022.115402

Isukuru, E. J., Opha, J. O., Isaiah, O. W., Orovwighose, B., and Emmanuel, S. S. (2024). Nigeria's water crisis: abundant water, polluted reality. *Clean. Water* 2, 100026. doi:10.1016/j.clwat.2024.100026

Jiang, Z.-Y., Sun, X.-P., Luo, Y.-Q., Fu, X.-L., Xu, A., and Bi, Y.-Z. (2024). Recycling, reusing and environmental safety of industrial by-product gypsum in construction and building materials. *Constr. Build. Mater.* 432, 136609. doi:10.1016/j.conbuildmat.2024.136609

Jin, J., Chen, Y., Li, M., Liu, T., Qin, Z., Liu, Q., et al. (2024). Preparation of self-consolidating cemented backfill with tailings and alkali activated slurry: performance evaluation and environmental impact. *Constr. Build. Mater.* 438, 137088. doi:10.1016/j.conbuildmat.2024.137088

Khan, M., and McNally, C. (2024). Recent developments on low carbon 3D printing concrete: revolutionizing construction through innovative technology. *Clean. Mater.* 12, 100251. doi:10.1016/j.clema.2024.100251

Kosar, K., de Salles, L. S., Sharifi, N. P., Vandenbossche, J., and Khazanovich, L. (2023). Onsite strength determination for early-opening decision making of high early strength concrete pavement. *J. Traffic Transp. Eng. Engl. Ed.* 10 (2), 291–303. doi:10.1016/j.jtte.2021.12.005

Kuoribo, E., Shokry, H., and Mahmoud, H. (2024). Attaining material circularity in recycled construction waste to produce sustainable concrete blocks for residential building applications. *J. Build. Eng.* 96, 110503. doi:10.1016/j.jobe.2024.110503

Liang, H., Bian, X., and Dong, L. (2024). Towards net zero carbon buildings: accounting the building embodied carbon and life cycle-based policy design for Greater Bay Area, China. *Geosci. Front.* 15 (3), 101760. doi:10.1016/j.gsf.2023.101760

Liu, Q., Hu, R., Hu, L., Xing, Y., Qiu, P., Yang, H., et al. (2022). Investigation of hydraulic properties in fractured aquifers using cross-well travel-time based thermal tracer tomography: numerical and field experiments. *J. Hydrology* 609, 127751. doi:10.1016/j.jhydrol.2022.127751

Muauz, A., Behailu, B., and Bediru, H. (2024). Application of surface geophysical investigations and pumping test data analysis for better characterization of aquifer hydraulic parameters, Upper Awash Sub-Basin, Central Ethiopia. *J. Hydrology Regional Stud.* 55, 101933. doi:10.1016/j.ejrh.2024.101933

Pour, S. H., Wahab, A. K. A., Shahid, S., Asaduzzaman, M., and Dewan, A. (2020). Low impact development techniques to mitigate the impacts of climate-change-induced urban floods: current trends, issues and challenges. *Sustain. Cities Soc.* 62, 102373. doi:10.1016/j.scs.2020.102373

Pradel, M., Garcia, J., and Vaija, M. S. (2021). A framework for good practices to assess abiotic mineral resource depletion in Life Cycle Assessment. *J. Clean. Prod.* 279, 123296. doi:10.1016/j.jclepro.2020.123296

Rumbach, A., Sullivan, E., McMullen, S., and Makarewicz, C. (2022). You don't need zoning to be exclusionary: manufactured home parks, land-use regulations and housing segregation in the Houston metropolitan area. *Land Use Policy* 123, 106422. doi:10.1016/j.landusepol.2022.106422

Salami, B. A., Bahraq, A. A., Haq, M. M. U., Ojelade, O. A., Taiwo, R., Wahab, S., et al. (2024). Polymer-enhanced concrete: a comprehensive review of innovations and pathways for resilient and sustainable materials. *Next Mater.* 4, 100225. doi:10.1016/j.nxmate.2024.100225

Savinykh, V. V., Elansky, N. F., and Gruzdev, A. N. (2021). Interannual variations and long-term trends in total ozone over the North Caucasus. *Atmos. Environ.* 251, 118252. doi:10.1016/j.atmosenv.2021.118252

Shanmuganathan, R., Rath, B., Almoallim, H. S., Alahmadi, T. A., Jhanani, G. K., Lan Chi, N. T., et al. (2023). Utilisation of persistent chemical pollutant incorporating with nanoparticles to modify the properties of geopolymer and cement concrete. *Environ. Res.* 219, 114965. doi:10.1016/j.envres.2022.114965

Sharma, A. K., Sharma, M., Sharma, A. K., Sharma, M., and Sharma, M. (2023). Mapping the impact of environmental pollutants on human health and environment: a systematic review and meta-analysis. *J. Geochem. Explor.* 255, 107325. doi:10.1016/j.gexplo.2023.107325

Tamoor, M., Samak, N. A., and Xing, J. (2023). Life cycle assessment and policy for the improvement of net-zero emissions in China. *Clean. Eng. Technol.* 15, 100663. doi:10.1016/j.clet.2023.100663

Tiwari, A., Mahadik, K. R., and Gabhe, S. Y. (2020). Piperine: a comprehensive review of methods of isolation, purification, and biological properties. *Med. Drug Discov.* 7, 100027. doi:10.1016/j.medidd.2020.100027

Wang, H., Liu, T., Zhang, Z., Zou, D., Zhou, A., and Li, Y. (2024). Durability of SFCB reinforced low-alkalinity seawater sea sand concrete beams in marine environment. *Eng. Struct.* 317, 118616. doi:10.1016/j.engstruct.2024.118616

Wang, T., Tian, W., Lin, Y., Gou, X., Liu, H., Wang, X., et al. (2023). Decadal changes in the relationship between Arctic stratospheric ozone and sea surface temperatures in the North Pacific. *Atmos. Res.* 292, 106870. doi:10.1016/j.atmosres.2023.106870

Wu, L., Sun, Z., and Cao, Y. (2024). Modification of recycled aggregate and conservation and application of recycled aggregate concrete: a review. *Constr. Build. Mater.* 431, 136567. doi:10.1016/j.conbuildmat.2024.136567

Yan, T., Han, Q., Li, Z., Song, Y., Wang, Y., and Zhang, X. (2022). Influence of rare earth doping and calcination temperature on temperature sensitivity of gadolinium molybdate nanoparticle. *J. Alloys Compd.* 907, 164462. doi:10.1016/j.jallcom.2022.164462

Yang, B., Zhang, Y., Zhang, W., Sun, H., Wang, Q., and Han, D. (2024). Recycling lithium slag into eco-friendly ultra-high performance concrete: hydration process, microstructure development, and environmental benefits. *J. Build. Eng.* 91, 109563. doi:10.1016/j.jobe.2024.109563

Yu, Z., Wang, B., Li, T., Fan, C., and Yu, H. (2024). Effect and mechanism of activators on the properties of Yellow River sediment/fly ash/cement-based alkali-activated cementitious materials used for coal mine filling. *Constr. Build. Mater.* 445, 137955. doi:10.1016/j.conbuildmat.2024.137955

Yuan, S., Zhang, S., Pei, L., Liu, Y., Sun, Y., Peng, J., et al. (2024). Elaborating conspicuously low hydrogen permeability EVOH composite membrane upgraded by corrosion protection function. *J. Membr. Sci.* 708, 123050. doi:10.1016/j.memsci.2024.123050

Zaid, O., Alsharari, F., and Ahmed, M. (2024). Utilization of engineered biochar as a binder in carbon negative cement-based composites: a review. *Constr. Build. Mater.* 417, 135246. doi:10.1016/j.conbuildmat.2024.135246

Zhang, L., Song, Y., Shi, T., Zhao, Z., Zhang, X., Liu, Y., et al. (2024). A correlation study between the properties of manufactured sand and tunnel muck. *Case Stud. Constr. Mater.* 21, e03684. doi:10.1016/j.cscm.2024.e03684

Zhao, Y., Zhou, X., Zhou, Q., Zhu, H., Cheng, F., and Chen, H. (2024). Development of full-solid waste environmentally binder for cemented paste backfill. *Constr. Build. Mater.* 443, 137689. doi:10.1016/j.conbuildmat.2024.137689

Zhu, P., Chen, X., Liu, H., Wang, Z., Chen, C., and Li, H. (2024). Recycling of waste recycled aggregate concrete in freeze-thaw environment and emergy analysis of concrete recycling system. *J. Build. Eng.* 96, 110377. doi:10.1016/j.jobe.2024.110377